CrossMark

PATIENT FACING SYSTEMS

Two Automated Techniques for Carotid Lumen Diameter Measurement: Regional versus Boundary Approaches

Tadashi Araki[1] · P. Krishna Kumar[2,3] · Harman S. Suri[4,5] · Nobutaka Ikeda[6] ·
Ajay Gupta[7] · Luca Saba[8] · Jeny Rajan[2,3] · Francesco Lavra[8] ·
Aditya M. Sharma[9] · Shoaib Shafique[10] · Andrew Nicolaides[11] ·
John R. Laird[12] · Jasjit S. Suri[3,5,13] · Fellow AIMBE

Abstract The degree of stenosis in the carotid artery can be predicted using automated carotid lumen diameter (LD) measured from B-mode ultrasound images. Systolic velocity-based methods for measurement of LD are subjective. With the advancement of high resolution imaging, image-based methods have started to emerge. However, they require robust image analysis for accurate LD measurement. This paper presents two different algorithms for automated segmentation of the lumen borders in carotid ultrasound images. Both algorithms are modeled as a two stage process. Stage one consists of a global-based model using scale-space framework for the extraction of the region of interest. This stage is common to both algorithms. Stage two is modeled using a local-based strategy that extracts the lumen interfaces. At this stage, the algorithm-1 is modeled as a region-based strategy using a classification framework, whereas the algorithm-2 is modeled as a boundary-based approach that uses the level set framework. Two sets of databases (DB), Japan DB (JDB) (202 patients, 404 images) and Hong Kong DB (HKDB) (50 patients, 300 images) were used in this study. Two trained neuroradiologists performed manual LD tracings. The mean automated LD measured was 6.35 ± 0.95 mm for JDB and 6.20 ± 1.35 mm for HKDB. The precision-of-merit was: 97.4 % and 98.0 % w.r.t to two manual tracings for JDB and 99.7 % and 97.9 % w.r.t to two manual tracings for HKDB. Statistical tests such as ANOVA, Chi-Squared, T-test, and Mann-Whitney test were conducted to show the stability and reliability of the automated techniques.

Keywords Carotid artery · B-mode ultrasound · Lumen diameter · Scale-space · Classification · Region-based · Boundary-based · Level set segmentation

This article is part of the Topical Collection on *Patient Facing Systems*

✉ Jasjit S. Suri
jasjit.suri@atheropoint.com

1 Division of Cardiovascular Medicine, Toho University Ohashi Medical Center, Tokyo, Japan

2 Department of Computer Science and Engineering, National Institute of Technology Karnataka, Surathkal, India

3 Point-of-Care Devices, Global Biomedical Technologies, Inc., Roseville, CA, USA

4 Mira Loma, Sacramento, CA, USA

5 Stroke Monitoring and Diagnostic Division, AtheroPoint™, Roseville, CA, USA

6 Cardiovascular Medicine, National Center for Global Health and Medicine, Tokyo, Japan

7 Radiology Department, Brain & Mind Research Institute, Weill Cornell Medical College, New York, NY, USA

8 Department of Radiology, University of Cagliari, Cagliari, Italy

9 Department of Medicine, Division of Cardiovascular Medicine, University of Virginia, Charlottesville, VA, USA

10 CorVasc Vascular Laboratory, Indianapolis, IN, USA

11 Vascular Diagnostic Center, University of Cyprus, Nicosia, Cyprus

12 UC Davis Vascular Center, University of California, Davis, CA, USA

13 Department of Electrical Engineering, University of Idaho, Moscow, ID, USA

Introduction

Stroke is the second leading cause of disability, after dementia. Recent reports show that more than 15 million people globally suffer a stroke each year [1]. Stroke primarily occurs due to two reasons: (a) the blood supply to the brain is blocked due to stenosis in the lumen of the carotid artery or (b) the sudden rupture of a blood vessel within the brain [2]. The degree of luminal narrowing is considered as an indirect measure of the carotid atherosclerosis [3]. Accurate characterization of atherosclerotic luminal changes is therefore crucial in patient's diagnosis. Figure 1 illustrates the plaque formation in the carotid artery.

B-mode ultrasound imaging (US) is a non-invasive and inexpensive technique for the visualization and measurement of the carotid arterial morphology [4–7]. The lumen diameter (LD) and stenosis is calculated using manual methods where the doctor or sonographer can put caliper-based points at the near lumen-intima (LI) and the far LI corresponding to the proximal and distal ends of the carotid artery. The LD is then measured as the distance between these points [8]. Manual measurement of LD is tedious and has poor inter- and intra-observer agreement [9]. Development of faster hardware and innovative algorithms in the recent years has made it possible to automatically compute the LD [5, 10, 11]. Due to better image reconstruction tools in ultrasound imaging, such as compound and harmonic imaging, it is now possible to image the carotid artery in real time [8, 12]. However, clearly work needs to be done for accurate lumen segmentation. We believe that in clinical application, carotid LD should be equally more significant than carotid intima-media thickness (IMT) [11]. This is because the plaque develops on both the sides (proximal and distal) of the carotid walls and carotid LD truly
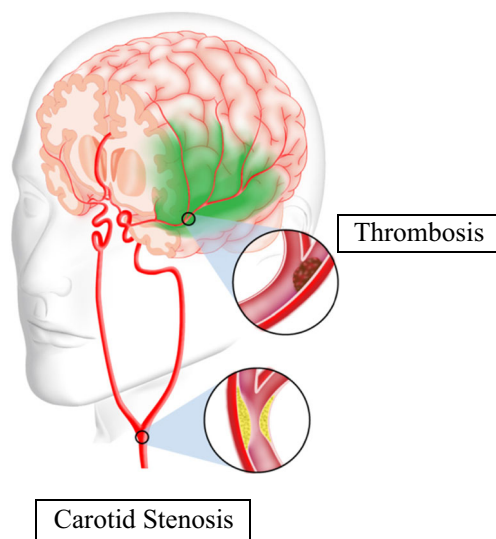

Fig. 1 Illustration of plaque formation leading to stenosis in the carotid artery (courtesy of AtheroPoint™, Roseville, CA, USA)

reflects a more comprehensive indicator of coronary artery disease (CAD) risk compared to carotid IMT.

Automated image-based methods for carotid lumen segmentation from US images are challenging due to the variability in data sets, such as: shape and size of carotid artery, occlusions caused by multi-focal plaques, arterial curvature, orientation of scanning probe, gain control during the acquisition, type of the transducer (linear vs. phased array), scanning protocol, and frequency of operation [5, 8, 11, 13, 14]. Furthermore, the non-uniform plaque growth at the interface of lumen and walls creates a challenge in the segmentation of the carotid artery because the image contrast depends on the composition and grade of the plaque [13]. Speckle noise level is another factor which affects the segmentation accuracy [5].

Several techniques have been attempted for carotid lumen segmentation, lumen boundary estimation, and lumen diameter measurement. We have classified these techniques into three categories [10, 15, 16] as: region-based [17, 18], boundary-based [19–22] or fusion-based [6].

Region-based techniques are not much explored in literature. In [17], the authors followed a global pixel classification strategy using the row-wise intensity distribution model from histograms to identify the lumen region from the carotid artery images. The main advantage of region-based strategy is that it is independent of gradient information which makes the segmentation robust to cases in which gaps exist in the boundaries of the carotid arteries. The major contribution of this paper is a region-based algorithm which uses the hypothesis that the blood has a constant density [23].

The boundary-based approaches or deformable models either follow parametric curves (traditional snakes) or geometric curves (level set) [24–28]. Manual initialization is required for snake based methods in a local neighborhood of the borders of the carotid artery. Moreover, since snake-based approaches rely on intensity gradients, they are often susceptible to false edges, and are sensitive to speckle noise and to gaps within the lumen borders. Even though few authors succeeded in carotid lumen segmentation, they provided no discussion about the quantification of LD.

Golemati et al. [19] used Hough's transform (HT) for the automated carotid lumen segmentation based on the assumption that straight lines (longitudinal images) and circles (transverse images) can be used for approximating the carotid lumen. However, this assumption may not be always valid, as the shape and orientation of the carotid arteries may vary depending on the acquisition procedure [6]. Further, Golemati et al. [19] suggests the use of active contours in combination with the Hough's transform technique for diseased arteries, where the arterial boundary departs from a simple geometrical shape. The aforementioned facts motivated us to develop a novel algorithm for carotid artery segmentation and LD measurement by combining the Hough's transform

with the level set approach. We use this method for benchmarking our region-based strategy.

This paper presents two different algorithms for automated segmentation of the lumen borders in carotid ultrasound scans. Algorithm-1 uses the region-based strategy, which is the key contribution of this study, while the algorithm-2 (boundary-based strategy) is presented for benchmarking. Both techniques are modeled as a two stage process: (i) global shape segmentation (or stage-I) for extraction of region of interest, and (ii) local shape extraction (or stage-II) of lumen interfaces (near LI and far LI corresponding to the near (proximal) and far (distal) walls of the carotid scans).

The layout of the paper is as follows: Materials and Methods provide background information on the material used for this study and explain the automated lumen segmentation algorithms in detail. Results section presents the experimental results on two different databases including performance evaluation of the two techniques. Discussion section presents the discussion on the results and the paper concludes in Conclusion.

Materials and methods

Patient demographics and data acquisition

Japan database (JDB)

Two hundred and two patients left and right common carotid artery (CCA) (404 Images) B-mode ultrasound images were retrospectively analysed (ethics approval and IRB granted, Toho University, Japan). Informed consent was obtained from all individual participants included in the study. There were 155 males (76.7 %) and 47 females (23.3 %) with mean age 67 and 75 years, respectively. These patients had a mean HbA1c of 6.28 ± 1.1 (mg/dl), Glucose 108 ± 31 (mg/dL), LDL cholesterol 101.27 ± 31.6 (mg/dl), HDL cholesterol of 50.26 ± 14.8 (mg/dl) and total cholesterol of 175.04 ± 38 (mg/dl). Two trained observers (Neuro radiologists with 10 years of experience) manually traced the lumen diameter borders.

The ultrasound scanner (Aplio XV, Aplio XG, Xario, Toshiba, Inc., Tokyo, Japan) used to examine the carotid arteries, was equipped with a 7.5-MHz linear array transducer. Same experienced sonographer (16 years of experience) had performed all the scans. The data were acquired in a time period ranging from July 2009 to August 2010. In this database, the vertical resolution was 0.05 ± 0.01 mm/pixel.

Hong Kong database (HKDB)

There were 50 subjects with a total of 300 images (6 ultrasound scans per patient, 3 scans each side of the neck showing three different acquisition scans: anterior, anterolateral and posterolateral approaches with simultaneous ECG gating). These subjects included asymptomatic postmenopausal Chinese women whose age ranged from 54 to 67 years. Informed consent was obtained from all individual participants included in the study. The mean age was 60.2 years. Of these 50 females (mixed pool), 28 females were abnormal (diseased) having following distribution: one was diabetic, three were hypertensive, 15 had hypercholesterolemia, seven had both hypertension and hyper cholestolemia, and two had all three abnormalities. The 22 normal (controls) females had normal blood pressure, total cholesterol and glucose levels in fasting blood. The carotid arteries were examined using a 13.5 MHz linear transducer of Sonoline Antares (Siemens, USA) ultrasound scanner. Each scan was digitally captured for 10 s and the digital dynamic clips of the six segments were archived for off-line analysis with the software Syngo.

Two trained observers (neuroradiologists with 10 years of experience) manually traced the lumen diameter borders in both the datasets using ImgTracer™ (AtheroPoint™, USA), a user-friendly commercial software [29] The observers have to choose 15 to 25 edge points proximal to the bulb depending upon the length of the carotid artery and the output will be ordered set of traced (x,y) coordinates.

Automated lumen segmentation system

We have modeled the segmentation algorithm as a two stage process. The motivation of the stage-I strategy comes from the fundamental reconstruction of the ultrasound image, where the distal (far) wall of the carotid artery has the brightest region [30]. This taps the information to build the global shape using scale-space framework [31, 32] combined with spectral analysis [33]. We analyze each column of the image pixels from bottom to top and identify the peaks and then, select the pair of peaks with high intensity value separating a pool of very small intensity values. These pair of peaks corresponds to media-adventitia (MA) borders. The region between the two MA borders is the region-of-interest (ROI). The output of the global shape is the ROI in which the local proximal and distal walls will be searched for lumen delineation. Figure 2 shows the region of interest estimation of the global-shape extraction process.

The local-based processing is modelled into two sets of competing methods: (a) region-based and (b) boundary-based, where each technique when combined with the global-shape method yields its own independent method. Both regional and boundary-based models are shown in local stages (stage-II) in Fig. 2.

a. Region Based (Classification) Technique for Lumen Segmentation

Fig. 2 Overall block diagram of the lumen region segmentation. Region based approach uses a classifier whereas in the boundary based approach level set is employed to extract the lumen region
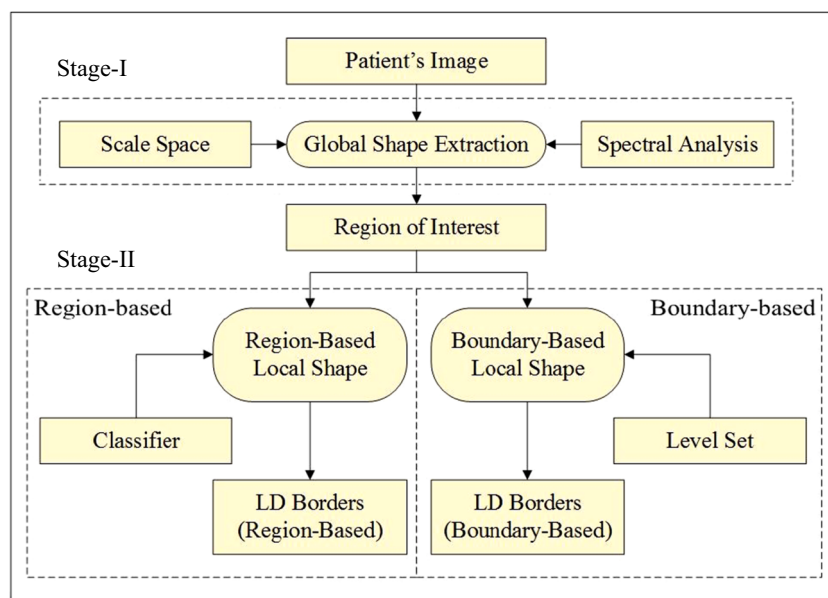
The region-based model captures lumen intensities under the constant blood density assumption [34]. This motivates the use of a statistical-based classifier such as K-means classifier [33, 35]. The ROI region is first captured using the combination of scale-space with spectral analysis (global shape method). This ROI has three regions: (a) low intensity lumen region, (b) high intensity or brightest adventitia region and (c) medium intensity plaque region. Thus we adapt a K-mean classifier with three pre-defined classes. On application of K-mean classifier, which yield three regions and lumen region is selected and enveloped as the largest region in binary form. The proximal and distal lumen morphologic borders are then delineated which constitute the borders of the lumen. Finally, the LD is estimated using the Polyline distance metric [36, 37].

The overall work flow of region-based approach is illustrated for a single image in Fig. 3. Figure 3(a) shows the cropped image using the automated cropping technique. Figure 3(b) shows the points captured using the spectral analysis. Figure 3(c) shows the spline fitted adventitial borders (both near and far). Figure 3(d) shows the ROI inside the rectangle (global shape extraction). Figure 3(e) shows the binary lumen from the K-means classifier. Figure 3(f) shows the final region-based LD borders after spline fitting (local shape extraction).

b. *Boundary Based Approach* (*Level Set Based*) *for Lumen Segmentation*

The fundamental assumption in the boundary-based approach is the ability to track the walls of the interfaces during the cardiac cycle. Though, we are not tracking walls of the interfaces in this scope of study, but the boundary-based approach originates from the idea that edge-model can be adapted for tracking such wall borders. These edge borders can be parametric or geometric when tracked. We model the interface detection using geometric models-based so-called level sets [17, 38, 39]. The elementary idea is to represent the boundaries of the carotid artery using a level set function, the evolution of which is controlled by some partial differential equations (PDEs) [39]. The key advantage of level set is the ability to follow the morphologic edges of the interfaces. However, the challenge in the level set is that where should be the starting interface before the push-pull can stretch the geometric curves to the stable position. Several techniques can be used to compute the initial edges before level set can be applied. We adapted a simple method keeping the assumption that lumen region has nearly constant density. We need something which can approximate the border of the interfaces which can then be acted as a bounding box when using level set. This approximation can be achieved using Hough's transform. The Hough's transform will give small line segments which will constitute the area within which the level set can explore. Hence, the level set evolution is limited by the borders obtained from the Hough's transform.

The level set method used in this paper is based on the general DRLSE (Distance Regularized Level set Evolution) technique proposed by Li et al. [40]. In DRLSE, the regularity of the level set function is intrinsically maintained during the level set evolution which is derived as the gradient flow and minimizes certain energy functional. The advantage of using DRLSE method is that the distance regularization effect eliminates the need for re-initialization of the level set function and thereby avoids its induced numerical errors. The complete levels set formulation (LSF) is explained below. Let *I* be an

Fig. 3 Results of different algorithmic steps of region-based technique on a single image. **a** Cropped image, **b** bright adventitial border points detected using spectral analysis, **c** Spline fitted on these points to show the adventitial borders, **d** the resulting ROI is marked with a rectangle extracted using global-shape extraction system, **e** binary lumen obtained from the classifier in the ROI using local region-based system, (f) final lumen borders after smoothing and spline fitting
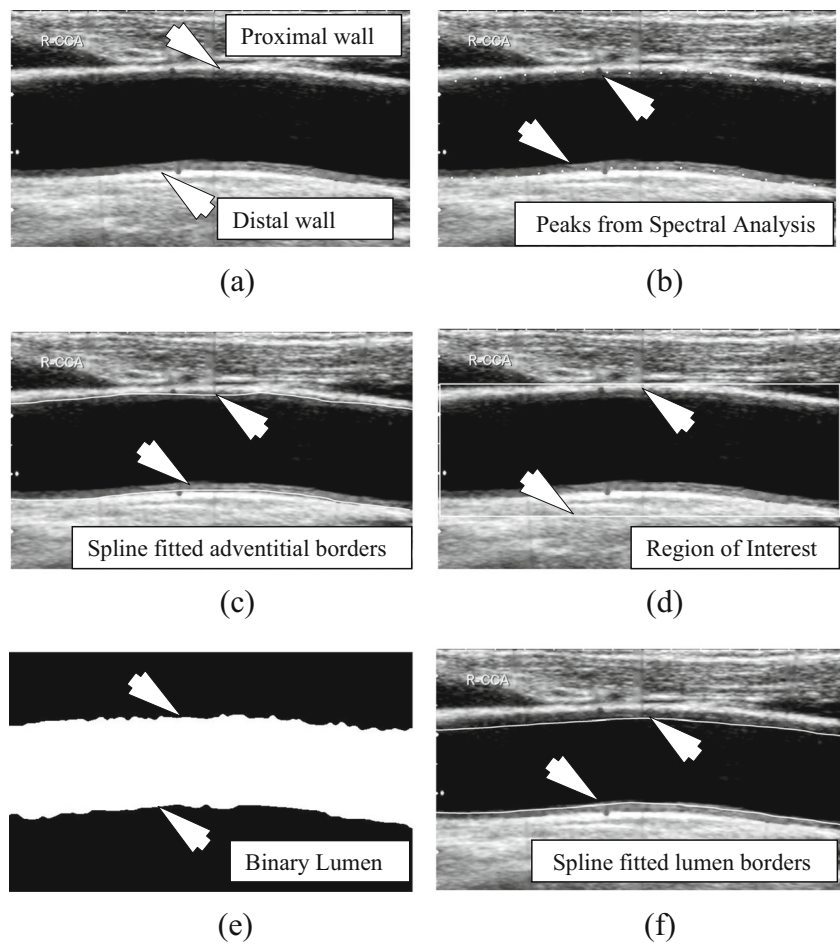
image on a domain Ω. Then the edge indicator function g can be defined as [40]:

$$g \triangleq \frac{1}{1 + |\nabla G_\sigma * I|^2} \tag{1}$$

where, ∇G_σ is a Gaussian kernel with a standard deviation σ. The convolution in Eq. (1) is used to smooth the image to reduce the noise. For an LSF $:\Omega \rightarrow \mathbb{R}$, we define an energy functional $\varepsilon(\Phi)$ by [40]:

$$\varepsilon(\Phi) = \mu R_p(\Phi) + \lambda L_g(\Phi) + \alpha A_g(\Phi) \tag{2}$$

where, μ is the coefficient of the distance regularization term $R_p(\Phi)$. $\lambda > 0$ and $\alpha \in \mathbb{R}$ are the coefficients of the energy functional $L_g(\Phi)$ and $A_g(\Phi)$, which are defined by [40]:

$$L_g(\Phi) \triangleq \int_\Omega g\delta(\Phi)|\nabla\Phi|dx \tag{3}$$

$$A_g(\Phi) \triangleq \int_\Omega gH(-\Phi)dx \tag{4}$$

where, δ and H are the Dirac delta function and the Heaviside function, respectively.

The level set evolution in Eq. (2) can be implemented by using the finite difference method provided in [40]. The iteration process used in the numerical implementation of DRLSE can be expressed as [40]:

$$\Phi_{i,j}^{k+1} = \Phi_{i,j}^k + \Delta t L\left(\Phi_{i,j}^k\right), \qquad k = 0, 1, 2.... \tag{5}$$

where the time dependent LSF $\Phi(x, y, t)$ is given in discretized form $\Phi_{i,j}^k$ with spatial index (i, j) and temporal index k. $L\left(\Phi_{i,j}^k\right)$ is the approximation of the right hand side in the evolution equations and Δt is the time step. The parameters used in the general DRLSE level set formulation [40] are given in the Table 1, choice of which was kept same for experiments on images in both the databases.

Figure 4 shows different algorithmic steps of boundary-based technique illustrated on a single image. Hough's transform is used as an initialization step before applying level set. After obtaining the ROI, Hough's transform is used to approximate the lumen borders using straight lines. The Hough's transform will give small line segments which will constitute the boundary for the level set to explore (see Fig. 4c). This will

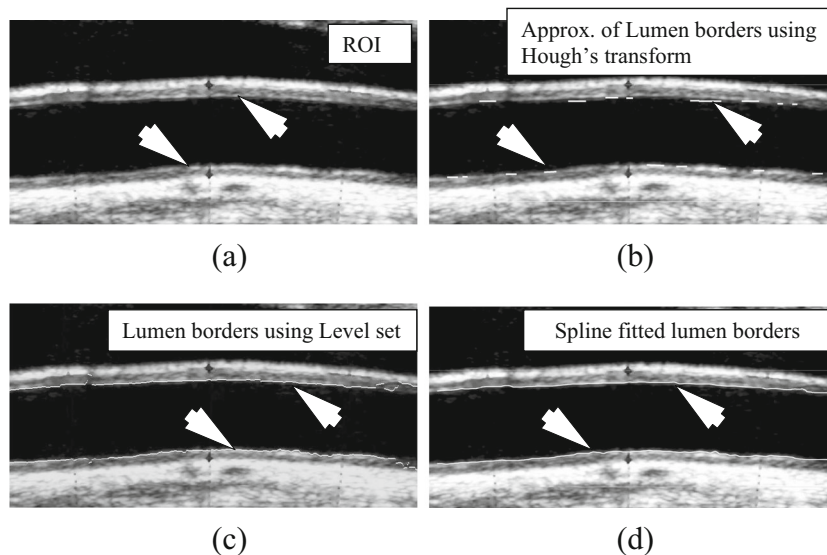**Table 1** Parameters used for the boundary-based (level set) segmentation

Parameter	Value
Time step (Δt)	1.0
Coefficient of the distance regularization term (μ)	0.2
Coefficient of the weighted length term (λ)	5.0
Coefficient of the weighted area term (α)	1.5
Parameter specifies the width of the Dirac Delta function (υ)	1.5
Scale parameter in Gaussian kernel (σ)	1.0

further increases the accuracy of the level set technique by avoiding the bleeding through the patches in the lumen interfaces.

Performance metrics

To evaluate the performance of our automated system, we have used the following statistical measures. Mean error and standard deviation shows the error and variation between the automated lumen diameter and manually traced diameter. Precision of merit (PoM) will provide similarity of mean automated lumen diameter with respect to the mean manual lumen diameter. Coefficient of correlation (CC) will give an idea about the closeness of the automated measurements with the manual expert tracings. The Bland-Altman plots will help in accurately determining the data distribution. Dice similarity (DS) and Jaccard index (JI) provides the relationship between the areas of manual and automated lumen segmentation regions. Further, T-test, Mann-Whitney test, ANOVA test and Chi-square test are performed to prove the statistical significance of the results. Statistical analysis was performed with the MedCalc 15.0 software (MedCalc, Belgium).

Results

Japan database

Table 2 compares automated lumen diameter against manual readings. This shows the closeness of the automated method against manual readings.

Figure 5 visually compares the results of both the methods. Left side shows the result of region-based (proposed) method and right side shows the result of boundary-based method. It can be seen that the region-based method outperforms the boundary-based technique.

HK database

Table 3 compares automated lumen diameter against manual readings. This shows the closeness of the automated method against the manual readings.

Figure 6 visually compares the results of both the methods. Left side shows the result of region-based (proposed) method and right side shows the result of boundary-based method.

Performance evaluation

Japan database

Figure 7 shows the scatter plot of automated LD against manual LD. The coefficient of correlation (CC) between the Auto LD and the two manual tracings for the region-based techniques are 0.91 ($p < 0.0001$) and 0.92 ($p < 0.0001$), respectively. Similarly, the CC between the Auto LD and the two manual LD's for the boundary-based techniques are 0.86 ($p < 0.0001$) and 0.85 ($p < 0.0001$), respectively. The Bland-Altman plots given in Fig. 8 give a much clear picture of the

Fig. 4 Results of different algorithmic steps of boundary-based technique on a single image. **a** ROI obtained using scale-space based global-shape extraction system; **b** Hough transform approximation of straight line borders; **c** lumen borders using the level set technique (local shape extraction); **d** final lumen borders after spline fitting

Table 2 Automated and manual mean lumen diameters

	Auto LD (mm)	Manual-1 LD (mm)	Manual-2 LD (mm)	PoM1 (%)	PoM2 (%)
Region-based	6.35 ± 0.95	6.19 ± 0.92	6.23 ± 0.95	97.4	98.0
Boundary-based	5.90 ± 0.97	6.19 ± 0.92	6.23 ± 0.95	95.3	94.0

Table 3 Automated and manual mean lumen diameters

	Auto LD (mm)	Manual-1 LD (mm)	Manual-2 LD (mm)	PoM1 (%)	PoM2 (%)
Region-based	6.20 ± 1.35	6.22 ± 1.37	6.33 ± 1.38	99.7	97.9
Boundary-based	5.43 ± 1.24	6.22 ± 1.37	6.33 ± 1.38	87.2	85.2

data including outliers. Cumulative frequencies of signed and unsigned Auto LD errors against manual tracings were computed. The unsigned cumulative frequency shows the total number of measurements with less than a particular error value irrespective of the sign (positive or negative). It was found that above 90 % of the LD measurements were within 1 mm error compared to the manual tracings for the region-based technique, whereas only around 80 % of the LD measurements fell within the 1 mm error range for the boundary-based technique. Further, the maximum error value did not exceed 2 mm in any of the cases. The cumulative frequency is an important performance statistic which refers to the error in the automated system.

Mann–Whitney test

The Mann–Whitney test is a non-parametric statistical test of the null hypothesis. This test is performed to determine whether or not two samples come from the same population. The analysis of the automated and manual LD variables was performed using Mann-Whitney test for independent samples. Tables 7 and 8 in appendix shows detailed Mann-Whitney test results for region-based and boundary-based techniques, respectively.

T- test

T-test was performed for independent samples to compare the means of two independent observations (automated and manual measurements). The null hypothesis is that the difference between the means of automated and manual measurements is equal to 0. Tables 9 and 10 shows the results of T test for both the methods. Since the calculated P-values are greater than the conventional 0.05, the null hypothesis cannot be rejected and the conclusion is that the two means do not differ significantly.

Fig. 5 **a** and **b** shows the visual comparison of the results using region-based and boundary-based methods. Left side shows the result of region-based (proposed) method and right side shows the result of boundary-based method. Auto lumen borders are marked in *solid white*, while manual lumen borders are shown in *dashed white*
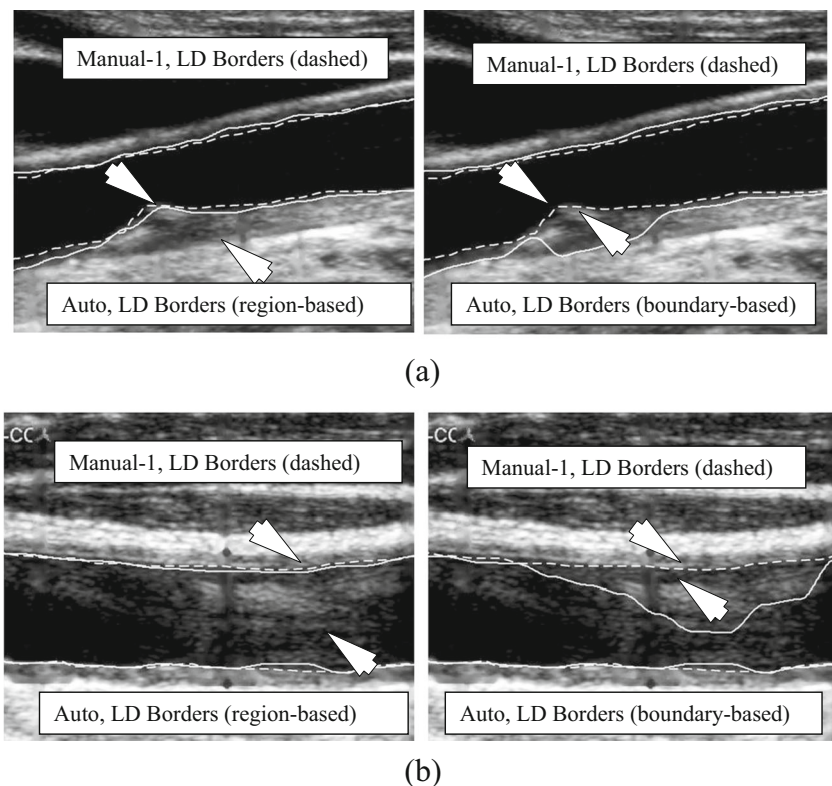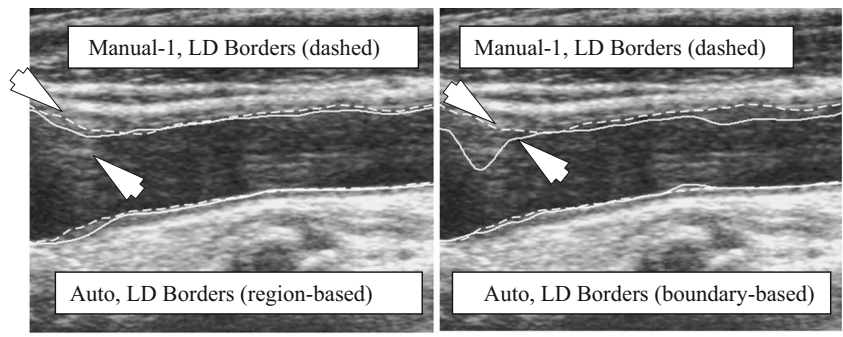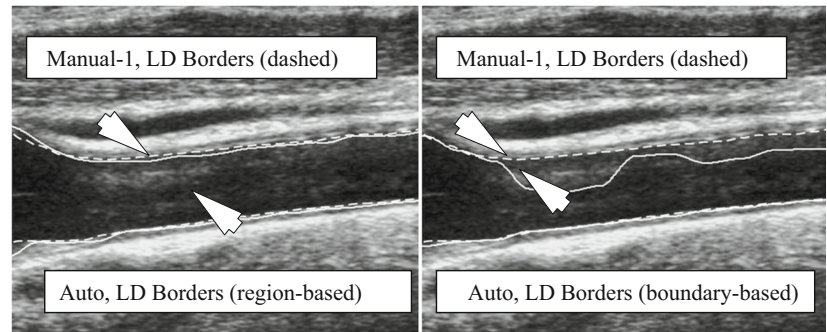

(a)

(b)

Fig. 6 **a** and **b** shows the visual comparison of the results of both the methods. Left side shows the result of region-based method and right side shows the result of boundary-based method. Auto lumen borders are marked in *solid white*, while manual lumen borders are shown in *dashed white*
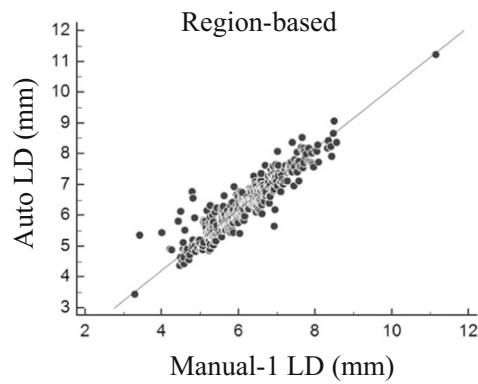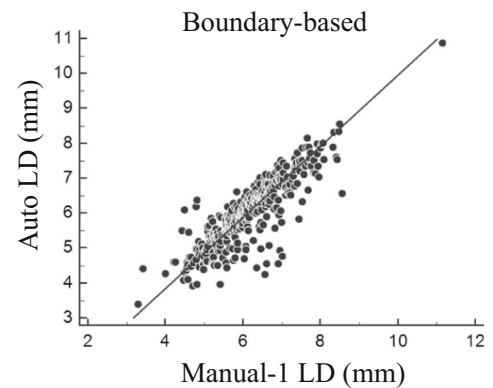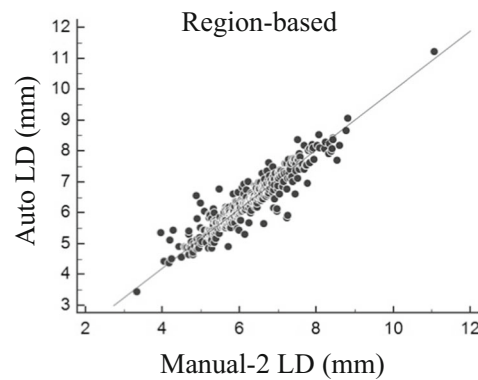

(a)

(b)

Fig. 7 **a** and **b** shows the scatter diagram for Auto LD against Manual-1 LD for the region-based and boundary-based techniques, respectively. Similarly, **c** and **d** shows the scatter diagram for Auto LD against Manual-2 LD for the region-based and boundary-based techniques, respectively
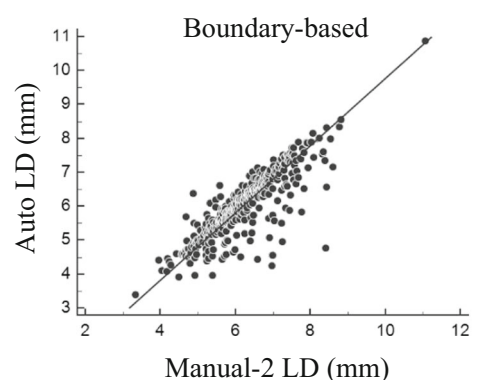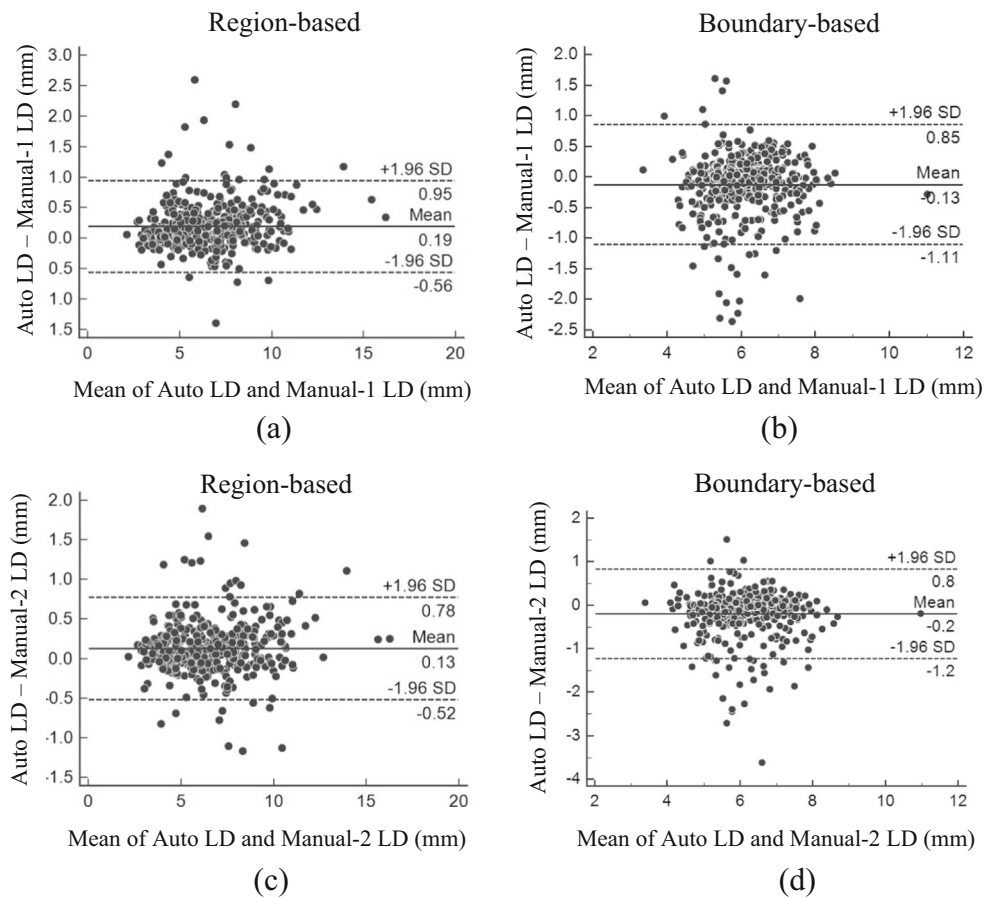

(a)

(b)

(c)

(d)

Fig. 8 **a** and **b** shows the Bland-Altman plots for Auto LD against Manual-1 LD for the region-based and boundary-based techniques, respectively. Similarly, **c** and **d** shows the Bland-Altman plots for Auto LD against Manual-2 LD for the region-based and boundary-based techniques, respectively

ANOVA test

ANOVA (one-way analysis of variance) is used to test the difference between the means of automated and manual measurements. The null hypothesis is that both the automated and the manual measurements have the same mean. We have performed the test at level of significance, 0.05. If, $P > 0.05$, we accept the null hypothesis or else, we reject the null hypothesis. The results of ANOVA test are given in Tables 11 and 12. Since the calculated P-value for LD is greater than 0.05, there is a statistically significant relationship between the auto (Auto LD) and the manual measurements (Manual-1 LD and Manual-2 LD).

Chi-Square test

Chi-Square test is performed to analyses the difference between the automated and the manual measurements. The detailed test results are given in Tables 13 and 14 in appendix section. Since, the test results are not significant at $P < 0.05$; the automated measurements (Auto LD) are not significantly different from the respective manual measurements.

Dice similarity and Jaccard index

Table 4 shows the relation of lumen area according to Dice similarity and Jaccard index for both the methods. If both regions are equal, dice similarity is 1 or 100 %. Here, the Dice similarity of both the readings is closer to 100. From the table, the lumen area calculated by automated method is close to manual segmentation area, and Manual-1 shows slightly higher similarity compared to Manual-2. Further, when considering Jaccard index, Manual-1 shows higher similarity than Manual-2.

Table 4   Dice similarity and Jaccard index

	Auto vs. Manual-1	Auto vs. Manual-2
Region-based		
Dice similarity	91 %	92 %
Jaccard index	86 %	85 %
Boundary-based		
Dice similarity	84 %	85 %
Jaccard index	81 %	79 %

HK database

Figure 9 shows the scatter plot of automated lumen diameter against manual lumen diameters. The coefficient of correlation (CC) between the Auto LD and the two manual tracings for the region-based techniques are 0.94 ($p < 0.0001$) and 0.93 ($p < 0.0001$), respectively. Similarly, the CC between the Auto LD and the two manual tracings for the boundary-based techniques are 0.84 ($p < 0.0001$) and 0.83 ($p < 0.0003$), respectively. The Bland-Altman plots given in Fig. 10 will give a much clear picture of the data including outliers.

The cumulative frequency is an important performance statistics which refers the intensity of error in the automated system. Cumulative frequencies of signed and unsigned Auto LD errors against manual tracings were computed. It is found that above 90 % of the LD measurements were within 1 mm error compared to the manual tracings for the region-based technique, whereas only around 80 % of the LD measurements fall within the 1 mm error range for the boundary-based technique. Further, 100 % of the LD measurements fall within the 2 mm range for both the methods.
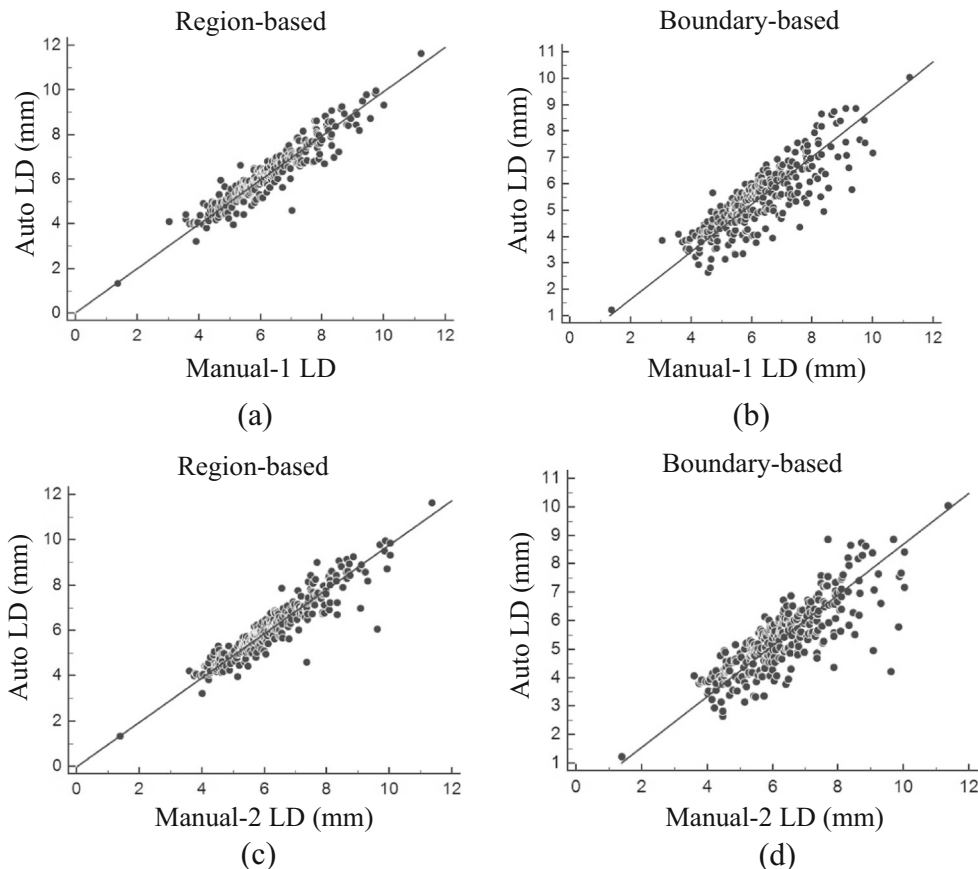
Mann-Whitney test

The analysis of the automated and manual LD variables was performed using Mann-Whitney test for independent sample. Tables 15 and 16 in appendix show Mann-Whitney test results for region-based and boundary-based techniques, respectively.

T- test

In order to check for differences between the manual and automated measurement, T-test was performed for independent samples. Tables 17 and 18 shows the results of T test for both the methods.

ANOVA test

We have performed the ANOVA test at level of significance, 0.05. If, $P > 0.05$, we accept the null hypothesis or else, we reject the null hypothesis. The results of ANOVA test are given in Tables 19 and 20. Since the calculated P-value for LD is greater than 0.05, there is a statistically significant relationship between the auto (Auto LD) and the manual measurements (Manual-1 LD and Manual-2 LD).

Fig. 9 **a** and **b** shows the scatter diagram for Auto LD against Manual-1 LD for the region-based and boundary-based techniques, respectively. Similarly, **c** and **d** shows the scatter diagram for Auto LD against Manual-2 LD for the region-based and boundary-based techniques, respectively

Fig. 10 **a** and **b** shows the Bland-Altman plots for Auto LD against Manual-1 LD for the region-based and boundary-based techniques, respectively. Similarly, **c** and **d** shows the Bland-Altman plots for Auto LD against Manual-2 LD for the region-based and boundary-based techniques, respectively

(a)　　(b)

(c)　　(d)
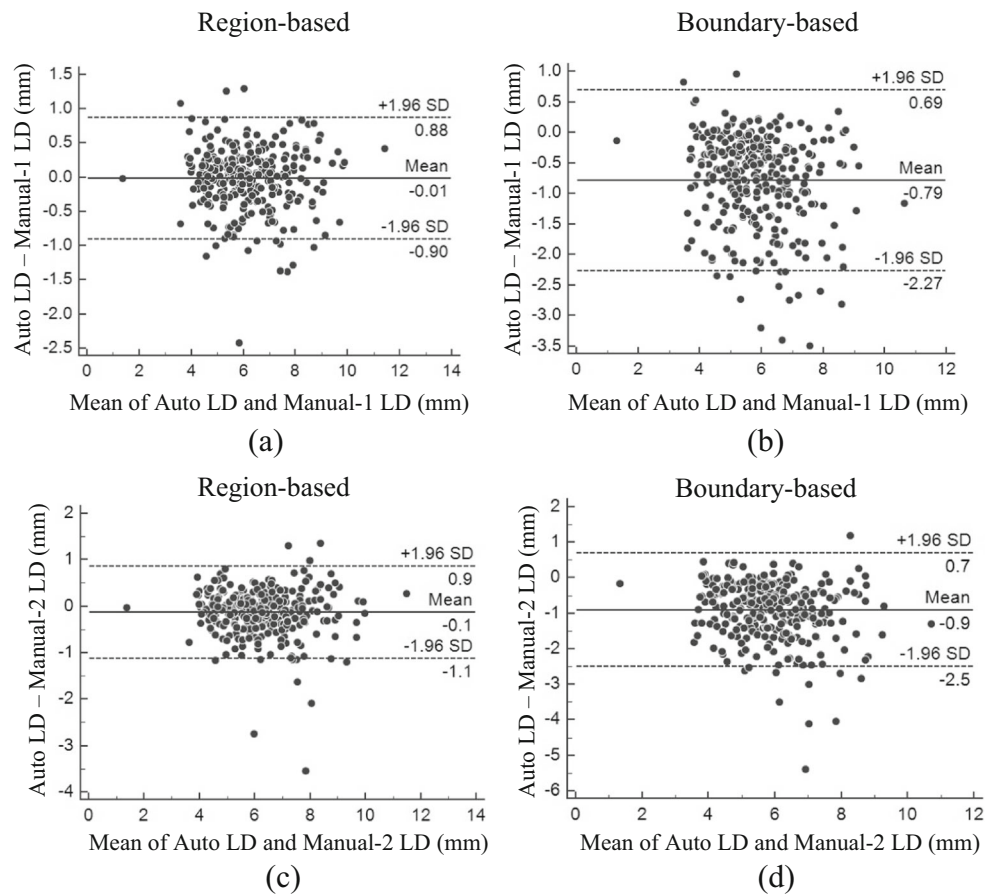
Chi-Square test

The detailed Chi-Square test results are given in Tables 21 and 22. Since, the test results are not significant at $P < 0.05$; the automated measurements (Auto LD) are not significantly different from the respective manual measurements.

Dice similarity and Jaccard index

Table 5 shows the relation of lumen area according to Dice similarity and Jaccard index for both the methods. From the table, the lumen area calculated by automated method is close

Table 5 Dice similarity and Jaccard index

	Auto vs. Manual-1	Auto vs. Manual-2
Region-based		
Dice similarity	94 %	92 %
Jaccard index	89 %	88 %
Boundary-based		
Dice similarity	85 %	83 %
Jaccard index	80 %	78 %

to manual segmentation area, and Manual-1 shows slightly higher similarity compared to Manual-2. Further, when considering Jaccard index, Manual-1 shows higher similarity than Manual-2.

Discussion

Automated system

The objective of this research was to design and develop two different algorithms for automated segmentation of the lumen borders from B-mode carotid ultrasound images. Performance of both algorithms was compared against the manual expert tracings. The system-based approach is novel and provides reliable, accurate, and validated clinical tool for lumen segmentation. It has a sound theoretical foundation and is driven by the requirements of the physicians and vascular radiologists which is an integral part of the clinical tool design. The main requirement is that the system must be fully automated from start to end and this is one of the reasons, we had to validate our system extensively with variability in data set and against the ground truth traced by the physicians.

We derived our concepts from the physics of ultrasound which yields the role of image reconstruction. Since the physics of ultrasound dictates that the far wall intensity to be highest with current ultrasound gain, frequency of attenuation, compound and harmonic imaging; we thus adapted a signal-based approach for detecting the location of the far wall in the B-mode ultrasound image [41]. The second aspect is that the anatomic structures which need to be segmented do not change on an average basis over the entire population. The scale-space concept to capture variable wall thickness during lumen segmentation is adapted for the first time. Further, the concept of capturing the global shape using the physics of ultrasound and spectral analysis prevents erroneous capture of walls such as jugular vein and other muscles which are floating around in the ultrasound image. Our database had variability on the wall thickness since our database consisted of women's data from Hong Kong and diabetic patients from Japan. By adjusting the σ value, we were able to capture the far wall adventitia region accurately. Figure 11 illustrates the variation of carotid artery images in the Japan database across different patients. Auto LD tracings using region-based technique on these images are given along with manual expert tracings.

One of the features which our system is based on is the hemodynamics of the fluid flow in the artery that is the blood. Sousa et al. [42] studied the link between hemodynamic behavior and stenosis pathophysiology based on clinical US examinations, and provided estimates of flow changes and forces at the c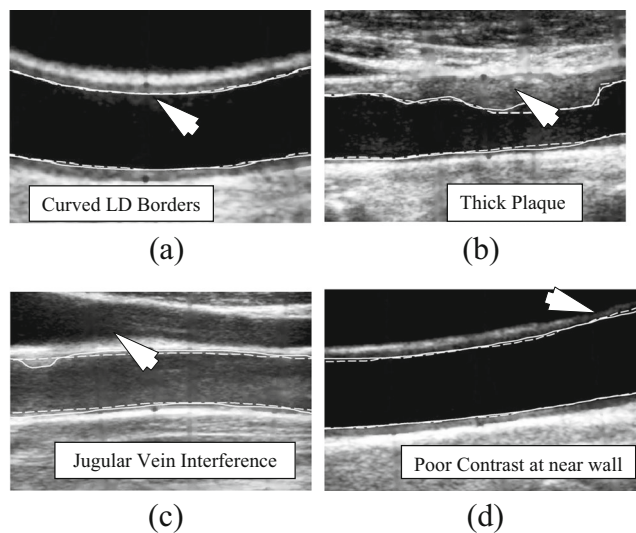arotid artery walls. In the current study, the concept of blood flow class constancy is used where blood flow is assumed to have fixed class intensity with least variation [43]. Using this property, we picked the flow pixels using pixel-based regional information under the statistical classifier framework. The interesting part is that we have carefully and intelligently applied these paradigms to avoid picking shadows due to calcium present in the near wall or poor image resolution in the lumen region.

We have adapted a mimicking approach which can mimic the calliper points along the lumen-intima interface (for near and far walls), and this will automatically give the LD. This mimicking approach can be best captured when the edges of the lumen-intima are captured. Since the lumen-interfaces have strong gradient edges in the presence of darker blood flow in ultrasound images, we need a model which can clamp the edges and follow the morphology of the plaque build-up. Thus we need a model which can capture both the morphology of the atherosclerotic disease and clamp the edges where it is supposed to be. The pioneering work of level set which culminated to capture the edges and morphology of the disease and we had extended such a model (so-called boundary based model) with improved characteristics both in terms of speed and complexity. This gives another novel framework for lumen segmentation and was utilized under benchmark paradigm. Note that, two objectives were met during this transition: (a) benchmarking process to compare regional-based approach against boundary-based approach and (b) provide a solid foundation to establish another system-based paradigm.

The experimental results on two different datasets illustrated the superior performance of the region-based strategy over the boundary-based strategy. This is due to the fact that, unlike region-based methods, boundary-based algorithms rely much on edges or image gradients. One explanation is that boundary-based methods are more sensitive to changes in gradient information at the edges of the wall during the cardiac cycle [44]. It is during this cardiac cycle, the image is frozen and processed for LD estimation. This sensitivity can be compensated for by taking neighbouring frames into consideration which is beyond the scope of the study. The second explanation for higher error is that atherosclerotic disease is multifocal and the plaque variations can be non-uniform along the carotid artery. Boundary-based techniques are sensitive to sudden changes in the variations of the grayscale intensity distribution along the common carotid artery, and will therefore yield less optimal results. This can be compensated for by taking regional statistics embedded with boundary-based information [15, 16].

One of the key applications of LD measurement is to understand the correlation between LD measurement and plaque score. Recently Saba et al. [45] has performed a comparative

Fig. 11 Illustrating the variation of carotid artery images across different patients in Japan database. **a** Curved lumen diameter (LD) borders; **b** High plaque deposit and narrowing of carotid artery; **c** Low contrast image with jugular vein interference. **d** Image having poor contrast difference at near wall. The *solid white* indicates the automated LD using region-based technique and the *dashed white* indicates the manual expert tracings

study of correlation between the carotid inter-adventitial diameter (IAD)/LD and the plaque score to predict the risk of stroke. Even though the plaque score has been correlated to IMT before [46], the novelty in this paper is the correlation of LD with the plaque score. The study by Saba et al. [45] used the scale-space based automated lumen diameter measurement system to accurately measure the carotid LD/IAD. However, the objective of the present study is completely different as we are comparing the performance of two different automated LD measurement systems.

Brief survey and benchmarking

Accurate knowledge and understanding of the geometry of the carotid arteries is important in their segmentation. Several automated algorithms have been proposed for the segmentation of the CCA, but majority of them are focused on the segmentation and measurement of the IMT. However, we have found that some authors pointed out the need for automated measurement of carotid lumen diameter [47–49]. The lumen segmentation algorithms have been classified into regional-based vs. boundary-based: region-based [17, 18], boundary-based [19–22]. Here, we describe each of these techniques and their limitations and discuss how they validated the measured parameters. Table 6 shows a comparative analysis of the carotid lumen segmentation techniques.

Golemati et al. [19] used a Hough transform for the automated lumen segmentation based on the assumption that the B-mode ultrasound images of longitudinal and transverse sections can be approximated using straight lines and circles, respectively. Though, they achieved a systolic LD accuracy of 98 % and diastolic LD accuracy of 97 %, this assumption may not be always valid, as the shape and orientation of the carotid arteries in the ultrasound scan may vary depending on the acquisition procedure. The authors tested their algorithm on just 10 subjects and the major weakness is the assumption that the vessels are straight which is not always true.

Molinari et al. [41] developed a completely automated IMT measurement system called carotid measurement using dual snakes (CMUDS): a class of AtheroEdge system (Global Biomedical Technologies, Inc., Roseville, CA). CMUDS was modeled as a dual parametric system corresponding to LI and MA borders with initialization from the far adventitia layer. The novelty of CMUDS was the first-order absolute moment–based external energy, which provided stable deformation. This system was evaluated on a multi-ethnic database of 665 longitudinal images and had achieved a success rate of 99.2 %. In another approach proposed by Molinari et al. [7], they proposed an automated method based on the assumption that the highest pixel intensities are in the far wall of the CCA. This methodology is patented which consisted of generating the composite image by registration. They used level-set-based algorithm followed by morphological image processing for lumen segmentation and the technique was evaluated on 200 CCA images. Since the above two methods were proposed for IMT measurement, we cannot compare their performance with the proposed technique.

The segmentation of carotid lumen region has been carried out by Santos et al. [17] based on binary image morphology, which utilized hypoechogenic characteristics of the lumen. This work also included a denoising step using an anisotropic diffusion filter to remove the speckle noise. The ROI was estimated using the method mentioned in the Golemati et al. [19]. They compared the area overlap between the auto and manual segmentation on 11 longitudinal US images and showed a mean area overlap of 96.78 %. Threshold-based region detection is always susceptible to false region estimation if the images are noisy due to low resolution or hyperechoic characteristics or shadows due to calcium in near wall. Further, the morphological processing operations are sensitive to noise and hence are not very stable.

The study by Loizou et al. [20] was concentrated on bifurcation region segmentation and diameter estimation through speckle reduction filtering and snake-based segmentation. This algorithm faced the challenge of initialization of snakes and did not give a high value of coefficient of correlation between their method and manual reading (CC = 0.63). Further, this algorithm was evaluated on just 20 images. Yang et al. [21] used an active shape-based model to segment both media-adventitia (MA) boundary and lumen-intima (LI) boundary on transverse views slices from three-dimensional ultrasound (3D US) images. This was a semi-automated method and was tested on a small database having 68 images form 17 patients. The authors have used the point distribution model to represent an object as a set of labeled points. However, no ROI was computed. The performance was evaluated against manual tracings. The method yielded a Dice similarity coefficient (DSC) of 94.4 % ± 3.2 % and 92.8 % ± 3.3 % for the media-adventitia-boundary (MAB) and lumen-intima-boundary (LIB), respectively. Yang et al. [8] method did not use longitudinal images in their study.

Lumen axis detection for carotid artery was discussed by Rocha et al. [22] using dynamic programming. They assumed that the CCA is the largest blood vessel nearest to the bottom of the image and the jugular vein will appear above the CCA. Even though the algorithm by Rocha et al. tested on 199 images and has got a success rate of 99.5 %, they did not attempt to measure the carotid LD. Their objective was limited to the detection of carotid lumen axis and not the measurement of any parameters. One of the main limitations of their study is that the near wall was not considered in their approach, since its visibility in 2D B-modes images is usually much worse than the far wall visibility. However, the measurement of lumen diameter requires the segmentation of near wall borders.

Table 6 Comparative analysis of the carotid lumen segmentation techniques

#	Author & year	Method	Auto/Semi-auto	# subjects	# images	Longitudinal vs. Transverse view	Performance (against manual tracings)
1	Golemati et al. (2007) [19]	Hough transform	Auto	10	Image sequences of length 70–80	Both	Systolic LD ACC: 98 % Diastolic LD ACC: 97 %
2	Molinari et al. (2011) [41]	Developed an inter-greedy technique to fuse two carotid wall boundaries	Auto	150	200	Longitudinal	NA
3	Molinari et al. (2012) [7]	Based on the hypothesis that the highest pixel intensities are in the far wall of the CCA	Auto	130	200	Longitudinal	NA
4	Santos et al. (2013) [17]	Anisotropic diffusion filter for speckle removal and morphologic operators are employed in the detection of the artery (used hypoechogenic characteristics of the lumen for binarization)	Auto	–	11	Longitudinal	Mean area overlapped: 96.78 %
5	Loizou et al. (2013) [20]	Snake based segmentation approach	Semi-Auto	20	20	Longitudinal	Auto LD: 5.77 ± 0.99 mm Manual LD: 5.59 ± 0.84 mm CC = 0.63 ($p = 0.001$)
6	Yang et al. (2013) [21]	Active Shape Model	Semi-auto	17	68	Transverse	NA
7	Rocha et al. (2014) [22]	Gaussian filtering and dynamic programming	Auto	25	199	Longitudinal	NA
8	Sifakis et al. (2014) [18]	Combination of anatomical knowledge and statistic	Auto	100	2149	Longitudinal	NA
9	Carvalho et al. (2015) [50]	Intensity joint-histogram classification and graph-based segmentation	Auto	17	21	Longitudinal	RMSE: 0.191 ± 0.043 mm and 0.351 ± 0.176 mm
10	Sharma et al. [51]	spectral analysis combined with pixel classification	Auto	202	404	Longitudinal	POM: 98.0 % and 99.0 %
11	Proposed Method	Scale-space combined with pixel classification and level set	Auto	202	404	Longitudinal	CC: 0.91 and 0.92 POM: 97.4 % and 98.0 %
				50	300	Longitudinal	CC: 0.94 and 0.93 POM: 99.7 % and 97.9 %

ACC Accuracy, *RMSE* Root Mean Square Error, *CC* coefficient of correlation, *PoM* Precision of Merit, *NA* Not Available

A user-independent, real-time algorithm is introduced by Sifakis et al. [18] for carotid artery localization in longitudinal B-mode ultrasound images. Their technique used basic image statistics along with arterial anatomical knowledge. They built their model with the assumption of three regions (brightest far wall region, darkest lumen, and then the second brightest near wall) in an ultrasound image. The method's evaluation and parameter value optimization were performed on a threefold cross validation basis. Even though the method proposed by Sifakis et al. [18] showed carotid artery segmentation, there was no discussion about the quantification of lumen diameter and benchmarking against gold standard. Recently, Carvalho et al. [50] proposed a method using simultaneously acquired B-mode ultrasound and contrast enhanced ultrasound image sequences. Their approach included motion estimation from image sequences and image registration. This work seemed to be quite different from the proposed approach. However, they used a graph based approach for the lumen segmentation.

Sharma et al. [51] presented AtheroEdge™ 2.0, a two stage process for automated carotid lumen diameter measurement. This method combines spectral analysis with pixel classification paradigm for LD measurement. The outputs of this clinical system were LD along with stenosis severity index (SSI). The algorithm was tested on 202 patients and achieved a precision-of-merit of 98.05 % and 99.03 % w.r.t to two observers. However, this system lacks a model-based approach for lumen segmentation.

The proposed method combines the scale-space paradigm with pixel classification as global and local models. This paper also benchmarks the current paradigm against a boundary-based approach where the global shape is extracted first followed by edge capturing using a level set paradigm. Further, we have tested our algorithm on a large database consisting of more than 700 images from 252 subjects. We got the POM values 99.7 % and 97.9 % and CC values 0.94 and 0.93 compared to manual tracings by experts which are quite good for an automated system. Hence we believe that our automated system has the potential to use in a clinical environment.

Strengths, weakness and extensions

Though our system is able to show promising results and has been well validated against manual tracings, we believe that there is a scope for improving the automated system. We have a plan to take out the curved vessels from the database and develop an improved system considering the curvature. Other possibilities include the application of any de-speckling technique before processing and multi-resolution analysis. Even though the proposed system showed high performance, as a future work, it can be tested on multi-ethnic databases from different countries. This will also help in improving the system by tackling more irregularities in the walls of the carotid artery.

Conclusions

We have presented two different algorithms for the automated lumen region segmentation and diameter measurement from B-mode ultrasound images. Both techniques are modelled as a two stage process. Stage one consisted of global-based model using scale-space framework combined with spectral analysis for extraction of the region of interest which is common for both algorithms. Stage two is modelled as a local-based strategy that extracts the lumen interfaces. The algorithm-1 is modelled as a region-based strategy using a multiclass framework, whereas the algorithm-2 is modelled as a boundary-based approach that uses the level set framework. Comprehensive statistical data analysis was performed to ensure the superior performance of the region-based technique against the two manual tracings. The region-based system showed high precision of merit and reliability. This image-based system for the automated lumen diameter measurement holds significant potential as a tool for stroke and cardiovascular risk stratification.

Appendix-A

Statistical analysis tables on Japan database

Table 7   Mann-Whitney test (Region-based technique)

	Manual-1	Manual-2	Auto
Median	6.1234	6.1839	6.3984
95 % CI for the median	6.0164 to 6.2641	6.0515 to 6.3234	6.2681 to 6.5180
Inter quartile range	5.5695 to 6.6957	5.6071 to 6.8252	5.7956 to 6.9969
Two-tailed probability	$P < 0.1502$	$P < 0.2328$	–

Table 8   Mann-Whitney test (Boundary-based technique)

	Manual-1	Manual-2	Auto
Median	6.1234	6.1839	6.0341
95 % CI for the median	6.0164 to 6.2641	6.0515 to 6.3234	5.8963 to 6.1912
Inter quartile range	5.5695 to 6.6957	5.6071 to 6.8252	5.4301 to 6.6210
Two-tailed probability	$P < 0.1677$	$P < 0.1080$	–

Table 9 Student's T- test (Region-based technique)

	Auto vs. Manual-1	Auto vs. Manual-2
Mean difference	−0.2640	−0.2000
Standard deviation of mean difference	0.3638	0.3397
Standard error of mean difference	0.01803	0.01684
95 % CI	−0.2994 to −0.2285	−0.2331 to −0.1669
Test statistic t	−14.640	−11.878
Degrees of Freedom (DF)	403	403
Two-tailed probability	P < 0.4784	P < 0.6461

Table 10 Student's T- test (Boundary-based technique)

	Auto vs. Manual-1	Auto vs. Manual-2
Mean difference	0.1291	0.1931
Standard deviation of mean difference	0.4989	0.5251
Standard error of mean difference	0.02473	0.02603
95 % CI	0.08047 to 0.1777	0.1419 to 0.2442
Test statistic t	5.220	7.418
Degrees of Freedom (DF)	403	403
Two-tailed probability	P < 0.4305	P < 0.3460

Table 11 ANOVA test (Region-based technique)

Groups	Count	Sum	Average	Variance
Manual-1 LD (mm)	404	2500.76	6.19	0.84
Manual-2 LD (mm)	404	2516.92	6.23	0.90
Auto LD (mm)	404	2565.40	6.35	0.90
ANOVA				
Source of Variation	SS	df	MS	F	P-value
Between Groups	3.156	2	1.5922	1.86	0.1510
Within Groups	824.433	949	0.83569		
Total	827.589	951			

SS um of square, *df* Degree of freedom (n-1 rule), *MS* Mean square (= SS / dof), F: (= Between Groups MS / Within Groups MS)

Table 12 ANOVA test (Boundary-based technique)

Groups	Count	Sum	Average	Variance
Manual-1 LD (mm)	404	2500.76	6.19	0.84
Manual-2 LD (mm)	404	2516.92	6.23	0.90
Auto LD (mm)	404	2383.60	5.90	0.94
ANOVA				
Source of Variation	SS	df	MS	F	P-value
Between Groups	3.456	2	1.5245	1.89	0.1241
Within Groups	810.956	940	0.79532		
Total	814.412	942			

SS Sum of square, *df* Degree of freedom (n-1 rule), *MS* Mean square (= SS / dof), F: (= Between Groups MS / Within Groups MS)

Table 13 Chi-Square test for LD (Region-based technique)

	Auto LD vs. Manual-1 LD	Auto LD vs. Manual-2 LD
Chi-squared	6.93	5.80
DF	9	9
Significance level	P = 0.6521	P = 0.7346
Contingency coefficient	0.636	0.590

DF Degrees of Freedom

Table 14 Chi-Square test for LD (Boundary-based Technique)

	Auto LD vs. Manual-1 LD	Auto LD vs. Manual-2 LD
Chi-squared	6.72	5.80
DF	9	9
Significance level	P = 0.6257	P = 0.5632
Contingency coefficient	0.773	0.673

DF Degrees of Freedom

Appendix-B

Statistical analysis tables on Hong Kong database (HKDB)

Table 15 Mann-Whitney test (Region-based technique)

	Manual-1	Manual-2	Auto
Median	6.0632	6.1904	6.0555
95 % CI for the median	5.8590 to 6.2108	5.9798 to 6.3344	5.8638 to 6.2583
Inter quartile range	5.3050 to 7.0678	5.3989 to 7.2619	5.1829 to 6.9867
Two-tailed probability	P < 0.8930	P < 0.5289	–

Table 16   Mann-Whitney test (Boundary-based Technique)

	Manual-1	Manual-2	Auto
Median	6.0632	6.1904	5.3746
95 % CI for the median	5.8590 to 6.2108	5.9798 to 6.3344	5.1415 to 5.5271
Inter quartile range	5.3050 to 7.0678	5.3989 to 7.2619	4.5613 to 6.1371
Two-tailed probability	*P* < 0.4673	*P* < 0.3505	–

Table 17   Student's T- test (Region-based technique)

	Auto vs. Manual-1	Auto vs. Manual-2
Mean difference	0.01172	0.1248
Standard deviation of mean difference	0.4528	0.5064
Standard error of mean difference	0.02606	0.02914
95 % CI	−0.03956 to 0.06299	0.06747 to 0.1822
Test statistic t	0.450	4.283
Degrees of Freedom (DF)	299	299
Two-tailed probability	*P* < 0.9533	*P* < 0.7951

Table 18   Student's T- test (Boundary-based Technique)

	Auto vs. Manual-1	Auto vs. Manual-2
Mean difference	0.7883	0.9014
Standard deviation of mean difference	0.7538	0.8123
Standard error of mean difference	0.04338	0.04674
95 % CI	0.7030 to 0.8737	0.8094 to 0.9934
Test statistic t	18.174	19.284
Degrees of Freedom (DF)	299	299
Two-tailed probability	*P* < 0.6033	*P* < 0.4572

Table 19   ANOVA test for LD (Region-based technique)

Groups	Count	Sum		Average	Variance
Manual-1 LD (mm)	300	1866		6.22	1.88
Manual-2 LD (mm)	300	1899		6.33	1.90
Auto LD (mm)	300	1860		6.20	1.82
ANOVA					
Source of Variation	SS	df	MS	F	*P*-value
Between Groups	2.642	2	1.2245	1.53	0.1502
Within Groups	622.302	784	0.65801		
Total	624.944	786			

SS Sum of square, *df* Degree of freedom (n-1 rule), *MS* Mean square (= SS / dof), F: (= Between Groups MS / Within Groups MS)

Table 20   ANOVA test for LD (Boundary-based technique)

Groups	Count	Sum		Average	Variance
Manual-1 LD (mm)	300	1866		6.22	1.88
Manual-2 LD (mm)	300	1899		6.33	1.90
Auto LD (mm)	300	1629		5.43	1.53
ANOVA					
Source of Variation	SS	df	MS	F	*P*-value
Between Groups	2.431	2	1.0125	1.48	0.1004
Within Groups	658.781	792	0.62971		
Total	661.194	794			

SS Sum of square, *df* Degree of freedom (n-1 rule), *MS* Mean square (= SS / dof), F: (= Between Groups MS / Within Groups MS)

Table 21   Chi-Square test for LD (Region-based technique)

	Auto LD vs. Manual-1 LD	Auto LD vs. Manual −2 LD
Chi-squared	5.25	5.79
DF	9	9
Significance level	*P* = 0.5879	*P* = 0.6037
Contingency coefficient	0.612	0.558

DF Degrees of Freedom

Table 22   Chi-Square test for LD (Boundary-based Technique)

	Auto LD vs. Manual-1 LD	Auto LD vs. Manual-2 LD
Chi-squared	6.03	6.33
DF	9	9
Significance level	*P* = 0.3269	*P* = 0.3577
Contingency coefficient	0.646	0.584

DF Degrees of Freedom

References

1. World Heart Federation 2015 [online]. Available at: http://www.world-heart-federation.org/cardiovascular-health/stroke/
2. Sobieszczyk, P., and Beckman, J., Carotid artery disease. *Circulation.* 114(7):e244–e247, 2006.
3. dev Sahu, C., and Wintermark, M., Clinical CT imaging of carotid arteries. In: *Multi-Modality Atherosclerosis Imaging and Diagnosis.* Springer, New York, pp. 123–128, 2014.
4. Suri, J.S., Kathuria, C., and Molinari, F. (Eds.), *Atherosclerosis disease management.* Springer Science & Business Media, New York, 2010.
5. Sanches, J.M., Laine, A.F., and Suri, J.S., *Ultrasound imaging.* Springer, New York, 2012.
6. Molinari, F., Zeng, G., and Suri, J.S., An integrated approach to computer based automated tracing and its validation for 200

common carotid arterial wall ultrasound images. *J. Ultrasound Med.* 29(3):399–418, 2010.

7. Molinari, F., Krishnamurthi, G., Acharya, U.R., et al., Hypothesis validation of far-wall brightness in carotid-artery ultrasound for feature-based IMT measurement using a combination of level-set segmentation and registration. *IEEE Trans. Instrum. Meas.* 61(4): 1054–1063, 2012.

8. Nicolaides, A., Beach, K.W., Kyriacou, E., et al., *Ultrasound and carotid bifurcation atherosclerosis.* Springer Science & Business Media, New York, 2011.

9. Saba, L., Montisci, R., Molinari, F., et al., Comparison between manual and automated analysis for the quantification of carotid wall by using sonography. A validation study with CT. *Eur. J. Radiol.* 81(5):911–918, 2012.

10. Suri, J.S., Wilson, D., and Laxminarayan, S., *Handbook of biomedical image analysis.* Vol. 2. Springer Science & Business Media, New York, 2005.

11. Saba, L., Sanches, J.M., Pedro, L.M., et al., *Multi-modality atherosclerosis imaging and diagnosis.* Springer, New York, 2014.

12. de Korte, C.L., Hansen, H.H., and van der Steen, A.F., Vascular ultrasound for atherosclerosis imaging. *Interface Focus.* 1(4):565–575, 2011.

13. Suri, J.S., Yuan, C., and Wilson, D.L., *Plaque imaging: pixel to molecular level.* Vol. 113. IOS Press, Amsterdam, 2005.

14. Bastida-Jumilla, M.C., Menchón-Lara, R.M., Morales-Sánchez, J., et al., Segmentation of the common carotid artery walls based on a frequency implementation of active contours. *J. Digit. Imaging.* 26(1):129–139, 2013.

15. El-Baz, A., Gimel'farb, G., and Suri, J.S., *Stochastic modeling for medical image analysis.* CRC Press, Boca Raton, 2015.

16. Suri, J.S., Singh, S., and Reden, L., Computer vision and pattern recognition techniques for 2-D and 3-D MR cerebral cortical segmentation (Part I): a state-of-the-art review. *Pattern Anal. Applic.* 5(1):46–76, 2002.

17. Santos, A.M.F., Tavares, J.M.R.S., Sousa, L., et al., Automatic segmentation of the lumen of the carotid artery in ultrasound B-mode images. *Expert Syst. Appl.* 40(16):6570–6579, 2013.

18. Sifakis, E.G., and Golemati, S., Robust carotid artery recognition in longitudinal B-mode ultrasound images. *IEEE Trans. Image Process.* 23(9):3762–3772, 2014.

19. Golemati, S., Stoitsis, J., Sifakis, E.G., et al., Using the Hough transform to segment ultrasound images of longitudinal and transverse sections of the carotid artery. *Ultrasound Med. Biol.* 33(12): 1918–1932, 2007.

20. Loizou, C.P., Kasparis, T., Spyrou, C., et al., Integrated system for the complete segmentation of the common carotid artery bifurcation in ultrasound images. *Artif. Intell. Appl. Innov.* 412(1):292–301, 2013.

21. Yang, X., Jin, J., Xu, M., et al., Ultrasound common carotid artery segmentation based on active shape model. *Comput. Math Methods Med.* 2013(11):3459–3468, 2013.

22. Rocha, R., Silva, J., and Campilho, A., Automatic detection of the carotid lumen axis in B-mode ultrasound images. *Comput. Methods Prog. Biomed.* 115(3):110–118, 2014.

23. Filardi, V., Carotid artery stenosis near a bifurcation investigated by fluid dynamic analyses. *Neuroradiol. J.* 26(4):439–453, 2013.

24. Farag, A., and Suri, J.S. (Eds.), *Deformable models: biomedical and clinical applications.* Vol. I. Springer Science & Business Media, New York, 2007.

25. Farag, A., and Suri, J.S. (Eds.), *Deformable models: biomedical and clinical applications.* Vol. II. Springer Science & Business Media, New York, 2007.

26. Suri, J.S., Liu, K., Singh, S., et al., Shape recovery algorithms using level sets in 2-D/3-D medical imagery: a state-of-the-art review. *IEEE Trans. Inf. Technol. Biomed.* 6(1):8–28, 2002.

27. Molinari, F., Meiburger, K.M., Saba, L., et al., Fully automated dual-snake formulation for carotid intima-media thickness measurement a new approach. *J. Ultrasound Med.* 31(7):1123–1136, 2012.

28. Molinari, F., Meiburger, K.M., Saba, L., et al., Constrained snake vs. conventional snake for carotid ultrasound automated IMT measurements on multi-center data sets. *Ultrasonics.* 52(7):949–961, 2012.

29. Saba, L., Lippo, R.S., Tallapally, N., et al., Evaluation of carotid wall thickness by using computed tomography and semi-automated ultrasonographic software. *J. Vasc. Ultrasound.* 35(3):136–142, 2011.

30. Molinari, F., Meiburger, K.M., Zeng, G., et al., Carotid artery recognition system: a comparison of three automated paradigms for ultrasound images. *Med. Phys.* 39(1):378–391, 2012.

31. Suri, J.S., Liu, K., Reden, L., et al., A review on MR vascular image processing algorithms: acquisition and prefiltering: part I. *IEEE Trans. Inf. Technol. Biomed.* 6(4):324–337, 2002.

32. Suri, J.S., Liu, K., Reden, L., et al., A review on MR vascular image processing: skeleton versus nonskeleton approaches: part II. *IEEE Trans. Inf. Technol. Biomed.* 6(4):338–350, 2002.

33. Araki, T., Banchhor, S.K., Londhe, N.D., et al., Reliable and accurate calcium volume measurement in coronary artery using intravascular ultrasound videos. *J. Med. Syst.* 40(3):1–20, 2016.

34. Prosi, M., Perktold, K., and Schima, H., Effect of continuous arterial blood flow in patients with rotary cardiac assist device on the washout of a stenosis wake in the carotid bifurcation: a computer simulation study. *J. Biomech.* 40(10):2236–2243, 2007.

35. Hartigan, J.A., and MA, W., Algorithm AS 136: A k-means clustering algorithm. *J. R. Stat. Soc.: Ser. C: Appl. Stat.* 28(1):100–108, 1979.

36. Suri, J.S., Haralick, R.M., and Sheehan, F.H., Greedy algorithm for error correction in automatically produced boundaries from low contrast ventriculograms. *Pattern Anal. Applic.* 3(1):39–60, 2000.

37. Molinari, F., Meiburger, K.M., Saba, L., et al., Ultrasound IMT measurement on a multi-ethnic and multi-institutional database: our review and experience using four fully automated and one semi-automated methods. *Comput. Methods Prog. Biomed.* 108(3):946–960, 2012.

38. Sethian, J.A., *Level set methods and fast marching methods: evolving interfaces in computational geometry, fluid mechanics, computer vision and materials science.* Cambridge University, Cambridge, 1999.

39. Suri, J.S., and Laxminarayan, S., *PDE and level sets.* Springer Science & Business Media, New York, 2002.

40. Li, C., Xu, C., Gui, C., et al., Distance regularized level set evolution and its application to image segmentation. *IEEE Trans. Image Process.* 19(12):3243–3254, 2010.

41. Molinari, F., Zeng, G., and Suri, J.S., Inter-greedy technique for fusion of different segmentation strategies leading to high-performance carotid IMT measurement in ultrasound images. *J. Med. Syst.* 35(1):905–919, 2011.

42. Sousa, L.C., Castro, C.F., António, C.C., et al., Toward hemodynamic diagnosis of carotid artery stenosis based on ultrasound image data and computational modeling. *Med. Biol. Eng. Comput.* 52(11):971–983, 2014.

43. Dey, N., Bose, S., Das, A., et al., Effect of watermarking on diagnostic preservation of atherosclerotic ultrasound video in stroke telemedicine. *J. Med. Syst.* 40(4):1–14, 2016.

44. Chow, T.Y., Cheung, J.S., Wu, Y., et al., Measurement of common carotid artery lumen dynamics during the cardiac cycle using magnetic resonance TrueFISP cine imaging. *J. Magn. Reson. Imaging.* 28(6):1527–1532, 2008.

45. Saba, L., Araki, T., Kumar, K.P., et al., Carotid inter-adventitial diameter is more strongly related to plaque score than lumen diameter: an automated tool for stroke analysis. *J. Clin. Ultrasound.* 44(4):210–220, 2016.

46. Saba, L., Ikeda, N., Deidda, M., et al., Association of automated carotid IMT measurement and HbA1c in Japanese patients with coronary artery disease. *Diabetes Res. Clin. Pract.* 100(3):348–353, 2013.

47. Polak, J.F., Sacco, R.L., Post, W.S., et al., Incident stroke is associated with common carotid artery diameter and not common carotid artery intima-media thickness. *Stroke.* 45(5):1442–1446, 2014.

48. Jensen-Urstad, K., Jensen-Urstad, M., and Johansson, J., Carotid artery diameter correlates with risk factors for cardiovascular disease in a population of 55-year-old subjects. *Stroke.* 30(8):1572–1576, 1999.

49. Godia, E.C., Madhok, R., Pittman, J., et al., Carotid artery distensibility a reliability study. *J. Ultrasound Med.* 26(9):1157–1165, 2007.

50. Carvalho, D.D., Akkus, Z., van den Oord, S.C., et al., Lumen segmentation and motion estimation in B-mode and contrast-enhanced ultrasound images of the carotid artery in patients with atherosclerotic plaque. *IEEE Trans. Med. Imaging.* 34(4):983–993, 2015.

51. Sharma, A. M., Araki, T., Kumar, A. M., et al. Ultrasound-based automated carotid lumen diameter/stenosis measurement and its validation system. *J. Vasc. Ultrasound* 2016 (in Press).